Journal of Experimental Botany, Vol. 59, No. 9, pp. 2513–2528, 2008
doi:10.1093/jxb/ern116

Journal of Experimental Botany
www.jxb.oxfordjournals.org

RESEARCH PAPER

Analysing the mechanical performance and growth adaptation of Norway spruce using a non-linear finite-element model and experimental data

T. Lundström[1,2,*], T. Jonas[1] and A. Volkwein[1]

[1] *WSL, Swiss Federal Institute for Snow and Avalanche Research SLF, 7260 Davos Dorf, Switzerland*

[2] *Laboratory of Dendrogeomorphology, University of Fribourg, 1700 Fribourg, Switzerland*

Received 14 December 2007; Revised 26 March 2008; Accepted 31 March 2008

Abstract

Thirteen Norway spruce [*Picea abies* (L.) Karst.] trees of different size, age, and social status, and grown under varying conditions, were investigated to see how they react to complex natural static loading under summer and winter conditions, and how they have adapted their growth to such combinations of load and tree state. For this purpose a non-linear finite-element model and an extensive experimental data set were used, as well as a new formulation describing the degree to which the exploitation of the bending stress capacity is uniform. The three main findings were: material and geometric non-linearities play important roles when analysing tree deflections and critical loads; the strengths of the stem and the anchorage mutually adapt to the local wind acting on the tree crown in the forest canopy; and the radial stem growth follows a mechanically high-performance path because it adapts to prevailing as well as acute seasonal combinations of the tree state (e.g. frozen or unfrozen stem and anchorage) and load (e.g. wind and vertical and lateral snow pressure). Young trees appeared to adapt to such combinations in a more differentiated way than older trees. In conclusion, the mechanical performance of the Norway spruce studied was mostly very high, indicating that their overall growth had been clearly influenced by the external site- and tree-specific mechanical stress.

Key words: Climate, critical load, mechanical optimisation, model performance and errors, stem taper, structural behaviour, thigmomorphogenesis.

Introduction

When a tree deflects, there is a change in the way loads, such as wind and snow, apply upon the tree. This phenomenon, which is called geometric non-linearity, is considered significant for a tree if the top deflection relative to height is larger than 20%. Until now, geometric non-linearity has rarely been fully considered in the mechanical analysis of flexible plants (Yang *et al*., 2005). In addition, trees also exhibit material non-linearity because they are composed of natural materials. This means that their mechanical properties depend on the magnitude of the load. Typically, the rotation of the root–soil system depends, in a non-linear way, on the applied turning moment of the root–soil system (Lundström *et al*., 2007*c*), just as the stem deflection due to bending depends on the applied bending stress (Lundström *et al*., 2008). These material non-linearities have never, to the author's knowledge, been considered in the analysis of tree mechanics. Consequently, it is not known which role they play in how a tree reacts to external load or under what conditions they may be mechanically advantageous for the tree, as they contribute to its flexibility.

Stresses in the tree stem and anchorage result from combinations of wind and snow load, and the overhanging weight of the leaning tree. The magnitude and frequency of such loads depend on the tree and stand characteristics, climate, and season. A sufficiently heavy load will cause the stem or the tree anchorage to fail. The type of failure depends on the stem and anchorage strengths, and on where and in which direction the load is applied. The magnitude of the failure load will, in addition, depend on how well the tree, including the crown, stem, and

* To whom correspondence should be addressed. E-mail: t.lundstroem@slf.ch

anchorage, has adapted its growth to the particular load combination (Telewski, 1995; Nicoll and Ray, 1996; Di Iorio *et al*., 2005). The most common failure mode of Norway spruce [*Picea abies* (L.) Karst.] is uprooting, but stem breakage may occur if the soil is frozen and if the crown is loaded with snow (Peltola *et al*., 1997, 2000). It is not clear to what extent a tree mutually adapts its stem and anchorage strengths to resist various types and combinations of natural loads.

Thigmomorphogenesis is the response of plants to mechanical stress (Jaffe, 1973; Telewski, 2006), with respect to their morphology and material properties (Chiatante *et al*., 2002). So far, most studies of thigmomorphogenesis have focused on isolated parts of the plant rather than on the plant as a whole (Moulia *et al*., 2006). Clearly, the spatial and temporal focus of such studies will affect how much detail they give in assessing and analysing the stress and growth histories of plants.

Wind-induced stem-bending stress has been the topic of several studies (Milne, 1991; Morgan and Cannell, 1994; Wood, 1995; Dean *et al*., 2002), where stress uniformity along the stem has been attributed to its taper. In addition to this geometric adaptation, the stem also adapts anatomically to mechanical stress through differential radial and apical growth (Meng *et al*., 2006). As the tree grows larger, this normally leads to stronger and stiffer wood forms along the lower, outer part of the stem (Ylinen, 1952; Niemz, 1993; Lundström *et al*., 2008), where the largest bending stresses due to wind are expected. Studying the thigmomorphogenesis of the stem, therefore, seems to require including both the taper and the material properties of the stem in the analysis.

This paper investigates how Norway spruce reacts to combinations of natural loading. For this purpose, a non-linear numerical tree model is provided with extensive experimental data. These data are first used to test the model performance. Then, on the basis of the model results, the stem thigmomorphogenesis is analysed with a novel method that considers both the taper and the material properties of the stem. The focus is on the mechanics of the tree as a whole, and the properties of growth were used to parameterize its mechanics. The findings are used to test three hypotheses: (i) a geometric and material non-linear analysis is required to reproduce *in situ* stem deflections and analyse critical loads; (ii) the strengths of the stem and the tree anchorage mutually adapt to the most frequent combination of seasonal tree-state and load; and (iii) the thigmomorphogenesis of the stem is the result of the prevailing combination of seasonal tree-state and load. Exploring these hypotheses should improve researchers' general understanding of how Norway spruce grows and thus contribute to the informed management of Norway spruce forests.

Materials and methods

Trees and sites

The selection of the 13 Norway spruces [*Picea abies* (L.) Karst.] analysed was intended to cover not only a range of frequent tree sizes and of typical growth conditions in the Alps (Schweingruber, 1996), but also a spectrum of different tree ages, social states, sites, and local stand densities. By taking into account these factors, it would be possible to analyse the tree growth response generally and spatiotemporally according to the mechanical loading. The site and tree characteristics relevant to this study are listed in Table 1. These, as well as all experimental data used in this study, have been obtained from plots used in winching tests (Kalberer, 2007; Lundström *et al*., 2007*b*, *c*). The standing tree is referred to with an (x, y, z)-coordinate system, with its origin (0, 0, 0) at the stem base, $z=H$ at the top of the tree, and x in the direction of the horizontal stem deflection. r is the radial distance from the pith, *DBH* the stem diameter over bark at breast height (z=1.3 m), and B the bark thickness. The symbols used in this paper are summarized in Table A1 in the Appendix.

Table 1. *Site and tree characteristics of the 13 spruces analysed*

Plot, local delimitation of the forest stand; *DBH*, stem diameter at breast height (1.3 m); H, tree height; L_C, crown length; z_{Cc}, height of the crown's area centre; AGE, cambial age; Social status (according to Dobbertin *et al*., 1997) in relation to neighbouring trees.

Plot no.	Tree no.	Elevation (m asl)	Exposition	Slope (°)	Stand density (trees ha^{-1})	*DBH* (cm)	H (m)	L_C/H (−)	z_{Cc}/H (−)	AGE at z=1.3 m (years)	Social status
1	11	1620	NE	35	1200	15	16	0.88	0.56	64	Dominated
2	12	1620	NE	35	800	15	15	0.86	0.53	47	Co-dominant
3	13	1780	ESE	31	500	22	21	0.76	0.57	103	Dominated
3	14	1780	ESE	31	500	35	26	0.80	0.56	118	Co-dominant
4	15	1650	NNW	33	500	44	32	0.57	0.68	177	Dominant
3	16	1780	ESE	31	500	52	33	0.87	0.51	267	Dominant
3	17	1780	ESE	31	500	58	35	0.82	0.52	271	Superior
5	21	460	NNW	4	350	19	17	0.82	0.56	28	Co-dominant
5	22	460	NNW	4	350	29	26	0.76	0.56	43	Co-dominant
6	23	620	NNE	5	250	40	36	0.44	0.77	85	Co-dominant
6	24	620	NNE	5	250	48	36	0.36	0.80	84	Dominant
7	25	620	NNE	5	120	65	40	0.60	0.67	83	Dominant
8	26	620	NNE	5	80	73	38	0.66	0.65	81	Dominant

The trees 11–17 (Table 1) had a mean $B(z{=}1.3\text{ m})/(DBH/2)$ of 7%. They grew at a high elevation (HE) on four closely situated plots (at about 46°46′ N, 9°49′ W) south of Davos, Switzerland. At these locations, the B-horizon (0.1 m<depth<0.4 m) is a dystric Cambisol. The 5:50:95% percentiles of daily temperature observed over the last 20 years are –8:+4:+15 °C and of 10-min-wind 0:2:6 m s^{-1}. The annual maximum 10-min-wind is 15 m s^{-1} and the annual precipitation 1100 mm. Almost half the precipitation falls as snow and there is snow cover for 6 months a year (MeteoSwiss, 2007. Climate database of the Swiss National Weather Service, http://www.meteoschweiz.ch/web/en/services/data_portal.html). The soil-frost depth generally increases from November to culminate with a mean:max depth of 0.25:0.75 m beneath the crown in April (Stadler *et al*., 1998; MeteoSwiss, 2007, http://www.meteoschweiz.ch/web/en/services/data_portal.html).

The trees 21–26 had a mean $B(z{=}1.3\text{ m})/(DBH/2)$ of 6%. They grew at a low elevation (LE) on four plots close to Zurich, Switzerland, with plots 5–6 at 47°14′ N, 8°53′ W and plots 7–8 at 47°22′ N, 8°28′ W. At these locations, the B-horizon (0.4 m<depth<1.0 m) is a dystric Cambisol with presence of Luvisol. Here, the 5:50:95% percentiles of daily temperature are –2:+10:+21 °C and of 10-min-wind 0:2:6 m s^{-1}. The annual maximum 10-min-wind is 22 m s^{-1}, and the annual precipitation 1150 mm. Almost 10% of the precipitation falls as snow and there is snow cover for about 33 d a year (MeteoSwiss, 2007, http://www.meteoschweiz.ch/web/en/services/data_portal.html). The maximum soil-frost depth beneath the crown is less than 0.10 m (Stadler *et al*., 1998; MeteoSwiss, 2007, http://www.meteoschweiz.ch/web/en/services/data_portal.html).

Attribution of mechanical properties to the tree model

The tree is divided into a sufficient number of equally long elements for which the mechanical properties are specified. In this study 100 elements are used. These elements have the idealized shape of circular cylinders, because the stem diameter on bark (D) differed little in the x- and y-directions (2% on average). Each element is attributed a stem diameter under bark $D_{ub}(z)$, according to Table 2 using the following measured data: D in the x- and y-directions every per cent of H up to $z/H{=}0.20$, and then every metre up to H; B in the x- and y-directions at $z/H{=}0.05$ and at least two additional stem heights (in stem discs). Each element is further attributed a stem weight and a crown weight and diameter, which are polynomials of z based on measurements every metre of tree height.

Table 2. *Sequential steps in the parameterization of the stem diameter as a function of stem height*

D, stem diameter over bark; D_{ub}, stem diameter under bark; B, bark thickness. Step 4 is not used by the tree model, only to analyse stem morphology.

Step	Description
1	Polynomial fit of $D_x(z)$ and of $D_y(z)$ with a polynomial degree so that the fitting error is <1% for the 2/3 lower stem and <5% for the 1/3 upper stem (the resulting degree was >16).
2	Calculation of $B_x(z)$ and $B_y(z)$ using a 5-degree polynomial of $B(z)/D(z)$ (Laasasenaho *et al*., 2005) scaled with the measured B_x and B_y at $z/H{=}0.05$. The fitting errors at the additional $B(z)$-measurements were all within the limits of the absolute values at the corresponding heights in step 1.
3	Calculation of $D_{ubx}(z) = D_x(z) – 2B_x(z)$, $D_{uby}(z) = D_y(z) – 2B_y(z)$, and the geometric mean $D_{ub}(z) = (D_{ubx}(z)D_{uby}(z))^{0.5}$.
4	Calculation of the normalized stem diameter $D_{05}(z) = D(z)/D(z/H{=}0.05)$, in the x- and y-direction, as the geometric mean, under and over bark.

Here, the crown diameter is the geometric mean of the extensions in the x- and y-directions. The stem-section elements are finally given the following deformation properties: a bending stress as a non-linear function of bending strain and stem height $\sigma(\varepsilon, z)$ (Equation 1, an approximation) and a shear stress as a non-linear function of shear strain $\tau(\gamma)$ (Equation 2, a simplification):

$$\sigma(\varepsilon, z) = \left(\overline{\frac{\sigma(\varepsilon)}{\sigma_{max}}}\right) \times \left(\overline{\frac{\sigma_{max}(z)}{\sigma_{max}(0.05H)}}\right) \times \sigma_{max}(0.05H) \quad (1)$$

$$\tau(\gamma, z) = \tau(\gamma) = \left(\overline{\frac{\sigma(\varepsilon)}{\sigma_{max}}}\right) \times \tau_{max} \quad (2)$$

where σ_{max} is the bending strength of the stem cross-section (sometimes called the modulus of rupture) and τ_{max} is the shear strength of the stem section (Table 3). The first two factors in Equation 1 are normalized mean (roof sign) curves of $\sigma(\varepsilon)$ and of $\sigma_{max}(z)$, respectively (Lundström *et al*., 2007*a*, 2008). The stem base is flexibly clamped to the ground. The lower end of the lowest element (at $z{=}0$) is therefore attributed a resistive rotational moment M^0 as a non-linear function of the rotational angle ϕ (Equations 3 and 4):

$$M^0(\phi) = M^0_{max} \times \overline{M^0_n}(\phi_n) \quad (3)$$

With

$$M^0_n = \frac{M^0}{M^0_{max}}; \phi_n = \frac{\phi}{\phi(M^0_{max})} \quad (4)$$

where $\overline{M^0_n}$ is the mean $M^0_n(\phi_n)$-curve for spruces at the two elevations (Lundström *et al*., 2007*c*), M^0_{max} is the maximum of M^0 (sometimes called the anchorage strength), and $\phi(M^0_{max})$ is the ϕ at M^0_{max} (Table 3). The idealized M^0-shape, resulting from $\overline{M^0_n}$, was used instead of the measured M^0-shape in order to simplify and systemize the modelling. This approximation was tested to make sure it had no significant effect on the results.

All the parameters in Table 3 are measured values (winching experiments), except for σ_{max} and τ_{max}. The cross-sectional σ_{max} was calculated on the basis of the annual ring width RW and the knottiness Q between the pith (radius $r{=}0$) and the bark ($r{=}D_{ub}/2$) as variables in statistical-mechanical models (Lundström *et al*., 2007*a*, 2008). RW was scanned and measured digitally (WOODSCAN 4.5, Freiburg University, Germany) in stem discs, in eight azimuthal directions as a function of r, and then averaged at the same age. Q was measured manually in digital photos of the discs and averaged accordingly. Data on $RW(r)$ and $Q(r)$ were obtained from at least four discs cut from the stem between $z{=}0$ and $z{=}H$, in addition to the disc at $z{=}0.05H$. The values of σ_{max}, calculated on the basis of the $RW(r)$ and $Q(r)$ in these additional discs, differed little from the $\sigma_{max}(z)$-values obtained with Equation 1. The latter $\sigma_{max}(z)$-curves were therefore used throughout the analysis. The cross-sectional τ_{max} was estimated (Lundström *et al*., 2008) on the basis of the mean RW of the inner 75% radial part of the stem cross-section (RW_i). RW_i was found to vary little with stem height, so $\tau_{max}(z)$ was set as a constant $= \tau_{max}(z{=}0.05H)$.

It is known that frost increases the strength and stiffness of moist wood and soil (Kollmann, 1968; Andersland and Ladanyi, 2004). Silins *et al*. (2000) showed that $MOE(z)$ of fresh wood increases by a factor ≈1.5. Trees winched in the winter at the HE-site (SLF, unpublished data) show that M^0_{max} increases by a factor ≈2.5. These factors were adopted to account for the frozen stem and soil.

Loads on the tree and combinations of tree state and snow load

In this study, intercepted snow provides the vertical load on the tree. Here, two nominal values of snow-water equivalent precipitation

Table 3. *Mechanical and growth characteristics of the trees analysed*

RW, annual ring width, where 'i' refers to the mean of the inner 75% radial part of the stem cross-section, and 'o' to the mean of the remaining outer radial part; ρ_w, bulk density, σ_{max}, bending strength, and τ_{max}, shear strength of the fresh stem. The other abbreviations are explained in the text.

Tree no.	M^0_{max} (KNm)	$\phi(M^0_{max})$ (°)	Values of the stem section at z=0.05H				
			RW_i (mm)	RW_o (mm)	ρ_w (kg m^{-3})	σ_{max} (MPa)	τ_{max} (MPa)
11	12	21.0	1.1	1.3	840	52.6	3.5
12	10	22.0	1.4	2.3	780	46.0	3.1
13	30	10.0	1.5	0.6	880	59.6	3.1
14	75	7.4	1.6	1.0	830	54.0	3.0
15	139	5.3	1.3	0.9	860	56.6	3.3
16	231	3.3	0.9	1.1	870	55.4	3.8
17	239	3.0	0.9	0.6	920	62.9	3.7
21	41	18.0	3.7	3.1	600	38.8	1.8
22	98	8.4	3.3	3.4	610	39.1	2.0
23	228	5.5	2.5	2.2	740	44.0	2.3
24	308	4.8	3.4	2.0	710	42.2	1.9
25	753	3.3	4.0	3.5	660	36.1	1.7
26	883	2.6	4.3	4.6	640	33.9	1.6

were first considered, SWE_{01}=20 and SWE_{02}=40 mm. The SWE effectively intercepted by the crown area projected on the ground was then calculated as $SWE = SWE_0 \times \pi/4 \times \text{atan}(\rho_{cv}/10)$, where ρ_{cv} is the vertical crown density = total crown mass/projected crown area on the ground, and 10 kg m^{-2} is the reference ρ_{cv}. This expression accounts for the fact that a denser crown has a better capacity to intercept snow (Strobel, 1978). The total snow loads on the crown, resulting from SWE_{01} and SWE_{02}, are denoted SL1 and SL2, respectively. They were distributed height-wise in proportion to the mass per height-section of the crown. This meant the top of the crown was attributed relatively more snow than its base because the crown density increased with height. SL1 was estimated to be the maximum amount of snow that can remain on the crown of a spruce of mean size when subjected to strong wind and SL2 the amount when there is almost no wind (Pomeroy and Gray, 1995; Bründl, 1997). The height-wise mean snow weight along the crown ranged between 6 kg m^{-1} and 48 kg m^{-1} for SL1 and between 12 kg m^{-1} and 95 kg m^{-1} for SL2.

The eight most significant combinations of seasonal tree state and snow load analysed are listed in Table 4, along with their probability of occurrence. Here, SL1 includes $10 \leqslant SWE_{01} < 30$ mm and SL2, $SWE_{02} \geqslant 30$ mm.

The lateral load, resulting from, for example, wind or snow pressure, was simplified and reduced to one concentrated force, $F(z)$. The next section describes how $F(z)$ was applied to the tree.

Tree model and model simulations

The tree model used is two-dimensional (Fig. 1). Since its single elements are one-dimensional, the forces and deformations along the stem, due to external forces, can be computed with the transfer matrix method. This method, which is based on the classical finite-element analysis of structural mechanics (Cook *et al*., 2002), is described in detail in Morgan and Cannell (1987) and Ancelin *et al*. (2004). In addition to the formulation in Morgan and Cannell (1987), the present method considers the geometric non-linearity and the material non-linearity of the deflecting tree.

The two non-linearities are taken into account by repeatedly performing the transfer matrixes method in its linear form, in an iterative process, until the tree model achieves static equilibrium. The geometry non-linearity is considered by redefining, at each repetition and by simple trigonometric transformation, the local coordinates (x', z') of each element in the global coordinates (x, z) in which the external forces act. Similarly, the material non-linearity is considered by redefining, at each iterative step, the secant-modulus of bending elasticity $E(\varepsilon) = \sigma(\varepsilon)/\varepsilon$ (cf. Equation 1) and of shearing elasticity $G(\gamma) = \tau(\gamma)/\gamma$ (cf. Equation 2) of the elements, to fit the $\sigma(\varepsilon)$ and the $\tau(\gamma)$ acting on the element. Here, the element deflection $dx'(z')$ due to the shear force (V, Fig. 1) is calculated with the mean shear stress of the cross section:

$$\bar{\tau}(z') = \frac{k}{A(z)} \times V(z') \tag{5}$$

as $\tau(\gamma, z')$ in Equation 2. This yields $\gamma(z')$ and thus:

$$dx'(z') = \gamma \times (z') \times dL \tag{6}$$

where k=1.1 is a shape factor for a circular cross-section to take into account the effective shear area, $A(z) = \pi D_{ub}(z)^2/4$ is the area of the cross-section, and dL is the length of one stem element. What is notable here is that the shear deformation of the stem due to asymmetrical stresses along the stem (dz'/dx') is very small compared to that due to the slip along the wood grain (dx'/dz'), and that therefore $\gamma \approx dx'/dz'$. The deformation along the stem is simply calculated with the stress-strain relationship in Equation 1, with the longitudinal stem stress = $N(z')/A(z)$ in place of σ and ε interpreted as the longitudinal stem strain, where N is the normal force (Fig. 1). The maximum shear stress within the cross-section is computed as $\tau(z', r=0) = 4/3 \times V(z')/A(z)$. The material non-linearity of the root–soil system is considered by redefining, at each iteration, its secant-stiffness = $M^0(\phi)/\phi$(Equation 3) to fit the M acting on the stem base. At the same time a small rotation is added or subtracted to the stem base, corresponding to a change in the stem base moment $M^0(\phi)$ to match the erroneous M at the tree top. The convergence criterion in the iteration to achieve a static equilibrium of the tree model is that the absolute values N, V, and M (Fig. 1) are all < 1E-06 (N and Nm) at the tree top.

On a second and a higher level of iteration, the critical lateral force $F_{crit}(z')$ that causes tree failure is sought. $F_{crit}(z')$ corresponds to the lower of the forces causing uprooting, i.e. $M^0 \approx M^0_{max}$, and stem breakage, i.e. $\sigma(\varepsilon, z') \approx \sigma_{max}(z')$. The corresponding static equilibriums are denoted StEq(M^0_{max}) and StEq(σ_{max}). The initial and estimated $F(z')$-value is set as a percentage of $M^0_{max}/z(F)$, to which a small value is then iteratively added or subtracted until the absolute values of $(M^0 - M^0_{max})/M^0_{max}$ or $(\sigma(\varepsilon, z') - \sigma_{max}(z'))/\sigma_{max}(z')$ are less than 5‰. To avoid model divergence, the $E = \sigma/\varepsilon$ at σ_{max} is used to calculate σ beyond σ_{max}. This is of no importance for the interpretation of the results other than that

Table 4. *Combinations of seasonal tree state and snow load in the model calculations*

HE, high elevation site; LE, low-elevation site. D_{ub} is the stem diameter under bark. SL and SWE are explained in the text.

Abbreviation		Description	Annual mean occurrence[a] (d)	
Tree state	Snow load		HE	LE
0		Normal	260	360
0	_SL1	Normal+snow load (SWE_{01})	45	5
0	_SL2	Normal+snow load (SWE_{02})	1	<0.1
FrSt		Frozen stem (depth >0.1D_{ub})	40[b]	0
FrSt	_SL1	Frozen stem+snow load (SWE_{01})	18[b]	0
FrSo		Frozen soil (depth >20 cm)	10[b]	0
FrStSo		Frozen stem and soil	7[b]	0
FrStSo	_SL1	Frozen stem and soil+snow load (SWE_{01})	2[b]	0

[a] Variations of up to ten times the mean occur for the abnormal combinations.
[b] Estimation based on Stadler *et al.* (1998) and Zweifel and Hasler (2000).

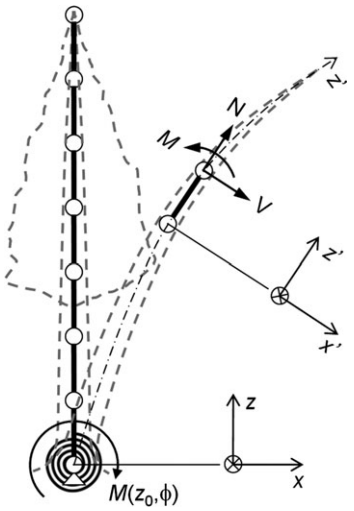

Fig. 1. The tree (grey dashed lines) and the model tree (heavy black lines) with schematic finite height segments of the tree. Each element is a one-sided clamped beam. For clarity, only one element of the deflected tree is shown with the moment (M) and forces (N, V) acting at its upper node. (x, z) refer to the global coordinate system and (x', z') to the local system of the element: z' ranges from 0 to H along the stem centre and x' is the sideway deflection of each element. $M^0(\phi)$ is the resistive moment of the root–soil system as a function of the rotational angle at the stem base.

$\sigma(z') > \sigma_{max}(z')$ indicates stem-bending failure. Figure 2 demonstrates typical model results at StEq(M^0_{max}) (Fig. 2A–D) and at StEq(σ_{max}) (Fig. 2E–H), which are here exemplified for two trees in an unfrozen state with no snow load.

Figure 2A–D shows tree no. 22 at StEq(M^0_{max}). The lateral force F is applied at z'/H=0.55 (Fig. 2A), which is close to the crown's area centre, z_{Cc} at z/H=0.56. F causes a total stem deflection (black line) and a stem deflection due to shearing only (grey line). The position of the initially applied force F_{init} (dashed line and arrow) differs from that of the converged solution F_{crit} (continuous line and arrow). Note that F is applied horizontally (in the x-direction) and at one fix z'-coordinate. For tree no. 22, uprooting occurs, i.e. the stem base moment $M^0(\phi)$ reaches M^0_{max} (Fig. 2B), before the stem fails, i.e. before the stem-bending stress $\sigma(z')$ reaches the stem-bending failure stress $\sigma_{max(z')}$ (Fig. 2C), where $\sigma(z')$ is the actual stress (solid line) and $\sigma_{max}(z')$ the failure stress (dashed line). The actual effective secant-modulus of elasticity of the stem section, $E(z') = \sigma(z')/\varepsilon(z')$ (Fig. 2D, continuous line), is, along the lower stem, lower than the modulus defined at $0.4\sigma_{max}(z')$, $MOE(z')$ (dashed line). The difference results from the non-linear $\sigma(\varepsilon,z)$ and means that the stem section softens while bending as $\sigma(z')$ approaches $\sigma_{max}(z')$, i.e. it bends more easily than $MOE(z')$ would predict.

Figure 2E–H shows tree no. 23 at StEq(σ_{max}). F is applied at z'/H=0.85 (Fig. 2E), just above z_{Cc} at z/H=0.77, and causes considerable stem deflections. In this example, the stem fails, $\sigma(z') \approx \sigma_{max}(z')$ (Fig. 2G), before the tree uproots, i.e. before $M^0(\phi)$ reaches M^0_{max} (Fig. 2F). The softening of the stem section while bending (Fig. 2H) is more extensive than in Fig. 2D.

The tree model was run for F_{crit} at the relative tree heights z'/H=0.10, 0.15, 0.20, …, 0.95, in order to determine the dependency of tree reactions on the height of the force application $z'(F_{crit})$. Here, all combinations of tree state and snow load (Table 4) were included to determine the dependency of tree reactions on the season.

To evaluate the model performance, the modelled and the measured stem deflections were compared at StEq(M^0_{max}), with F_{crit} at z'/H=0.20, for all trees in their normal state (Table 4).

Critical wind speed

The critical forces $F_{crit}(z'/H$=0.05, 0.10, …, 0.95) were interpolated every per cent of H up to 95%. F_{crit} at the height of the crown's area centre, z_{Cc} (cf. Table 1), was used to calculate the equivalent critical speed of steady wind, u_{crit}, with Equation 7:

$$F = C_D \times \frac{\rho \times u^2}{2} \times A_0;\ C_D = a + (1-a) \times e^{\alpha u} \qquad (7)$$

where C_D is the crown drag coefficient, A_0 is the horizontal projection of the undeformed crown, ρ is the density of air=1.17 kg m^{-3}, α=–0.09, and a=0.18 (Lundström *et al.*, 2007*b*). Snow on the crown is accounted for with $\alpha = \alpha/(1+\text{atan}(SWE/40))$, which is a hypothesis. Frozen branches are accounted for with $\alpha = \alpha 2/3$, as frozen wood is 50% stiffer (Silins *et al.*, 2000), which is applied when the stem is frozen (cf. Table 4). The two effects on α are multiplicative.

Stem thigmomorphogenesis

To analyse the degree to which the stem adapts its growth to mechanical stress (thigmomorphogenesis), the $\sigma(z')$ calculated by the model is compared with $\sigma_{max}(z')$. For this, a new formulation (Equation 8) was developed:

$$\eta(z'_1) = \left(SE \begin{pmatrix} z'_1 \\ z'=0 \end{pmatrix} \left(\frac{\sigma(z')}{\sigma_{max}(z')} \times \frac{\overline{\sigma_{max}(z')}}{\overline{\sigma(z')}} \right) \right)^{-1} \qquad (8)$$

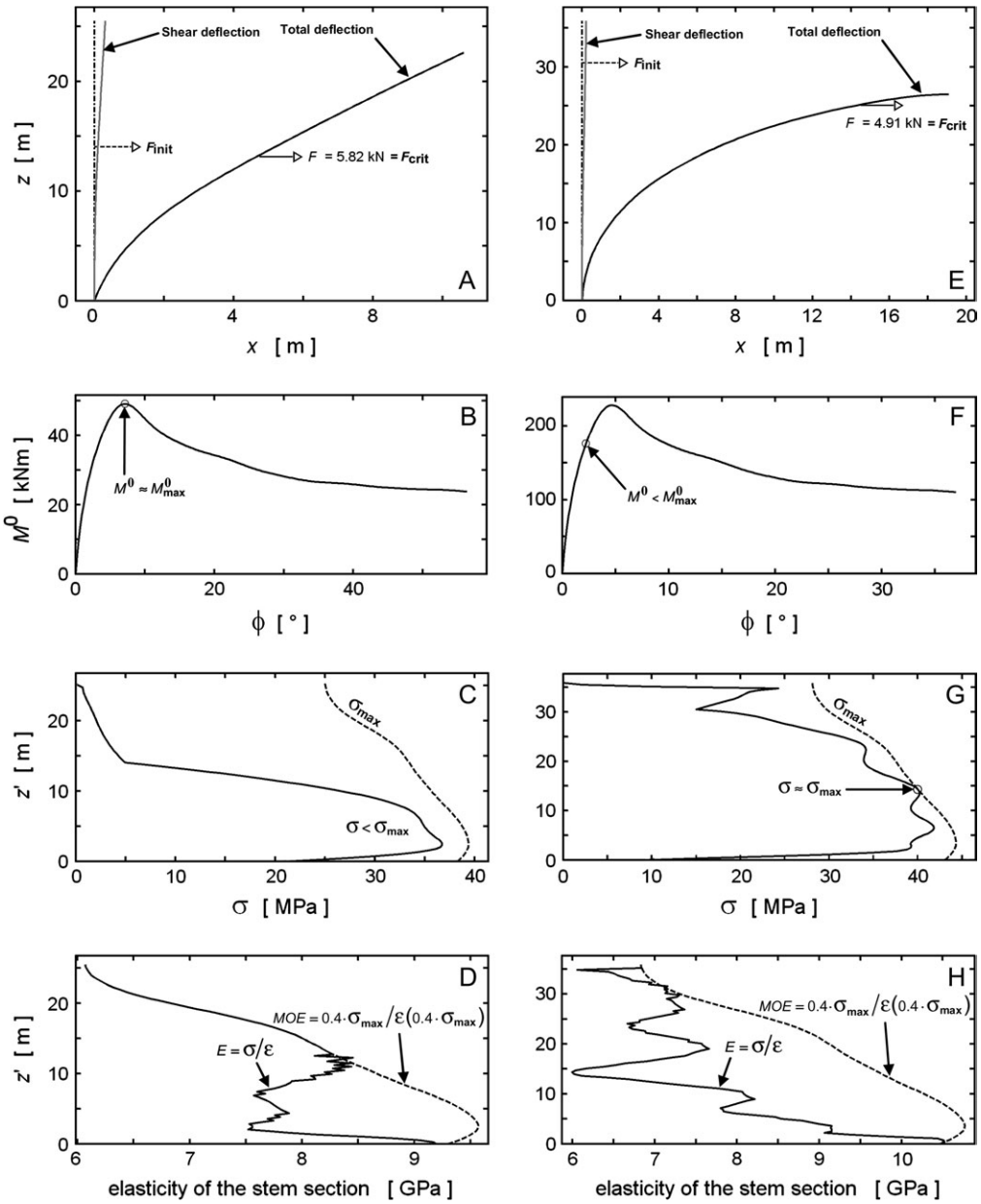

Fig. 2. Example of results with model convergence at StEq(M^0_{max}) (A–D) and at StEq(σ_{max}) (E–H). See text for explanations.

where η is the degree of uniform exploitation of bending stress capacity for the stem section between the stem base ($z'=0$) and the height of force application ($z' = z'_1$), SE is the standard error, $\sigma_{max}(z')$ is the bending strength (Table 3, Equation 1), and z'_1 is the (local) height coordinate of force application. Here, $\sigma(z')$ corresponds to the stem-bending stress at StEq(M^0_{max}) or StEq(σ_{max}). In principle, it would be more correct to use the most frequent stem stress. However, the most frequent values of $F(z'/H=0.05, 0.10, \ldots, 0.95)$, which correspond to the particular combinations of tree state and snow load, are *a priori* unknown. When the $\sigma(z')$ due to the mean wind speed was calculated and then magnified so that the shape of the $\sigma(z')$-curve could be compared with that of $\sigma(z')$ due to $F_{crit}(z_{Cc})$, it became apparent that the two $\sigma(z')$-shapes were almost identical (see the example given in the Results). The stem thigmomorphogenesis was therefore analysed using $\sigma(z')$ at StEq(M^0_{max}) or StEq(σ_{max}). It should further be noted that η is mathematically independent of the magnitude of σ_{max} and $\sigma(z')/\sigma_{max}(z')$, and that η measures the uniformity of exploitation of $\sigma_{max}(z')$ and not the magnitude of its exploitation.

Results

Model performance and potential sources of error when modelling stem deflections

The relative difference between modelled and measured horizontal tree-top deflection ranged from 1% (4 cm, tree 26) to 9% (45 cm, tree no. 22), averaging 3%. Since the exact rotation of the root–soil system was specified, these

discrepancies were due to errors in the parameterized flexibility of the stem only. Stem deflection could be modelled with very small errors up to the crown base. From here, small, local variations in flexibility accumulated or mutually balanced along the stem up to the tree top, with no sign of systematic errors. The errors in tree-top deflection were considered small and irrelevant compared to the other potential sources of errors outlined below, and the model performance was therefore fully acceptable.

Neglecting the geometric non-linearity means ignoring the additional moment resulting from the x-wise deflection of tree and snow weight, and therefore overestimating $F_{crit}(z)$. It also means ignoring the negative z-wise deflection of the leaning tree, which results in a shorter lever arm between the force application and the stem base, and therefore an underestimation of $F_{crit}(z)$. The net effect is an overestimation of $F_{crit}(z)$ if a geometric linear analysis is made. The overestimation for the trees with no snow load ranged from 5% (large tree) to 25% (small tree), averaging 14%. With snow on the crown, these values doubled and even tripled. In fact, some trees with snow-loaded crowns would have required almost no lateral force for tree failure to occur. This so-called unstable equilibrium would have been missed if the geometric non-linearity had been ignored.

Not accounting for the material non-linearity of the stem, i.e. using the stress-independent stem-bending elasticity $MOE(z)$ (the secant-modulus at $0.4\sigma_{max}$), leads to an underestimation of the stem-top deflection by between 0% and 19%, and on average by 8%. The relative softening of the stem in bending was typically a few per cent and reached locally up to 42%. If the non-linear resistive moment of the root–soil system is not taken into account, and instead a constant stiffness (the secant-stiffness at $0.4M^0_{max}$) is assumed in analogy to the stem section, then the tree-top deflection will be underestimated by a factor of between 5 and 7, and on average 6. If the tree deflections are underestimated, then $F_{crit}(z)$ will be overestimated. The net effects for material non-linearity are similar to those with geometric non-linearity. Hence, for trees with no snow load, the accumulated net effect of neglecting both material and geometric non-linearity in the analysis meant that $F_{crit}(z)$ was overestimated by between 7% (large tree) and 35% (small tree), and on average by 20%.

Tree reactions and critical loads: generalities

Figure 3 shows characteristic trends of the critical failure load F_{crit} and of tree reactions according to tree height. Up

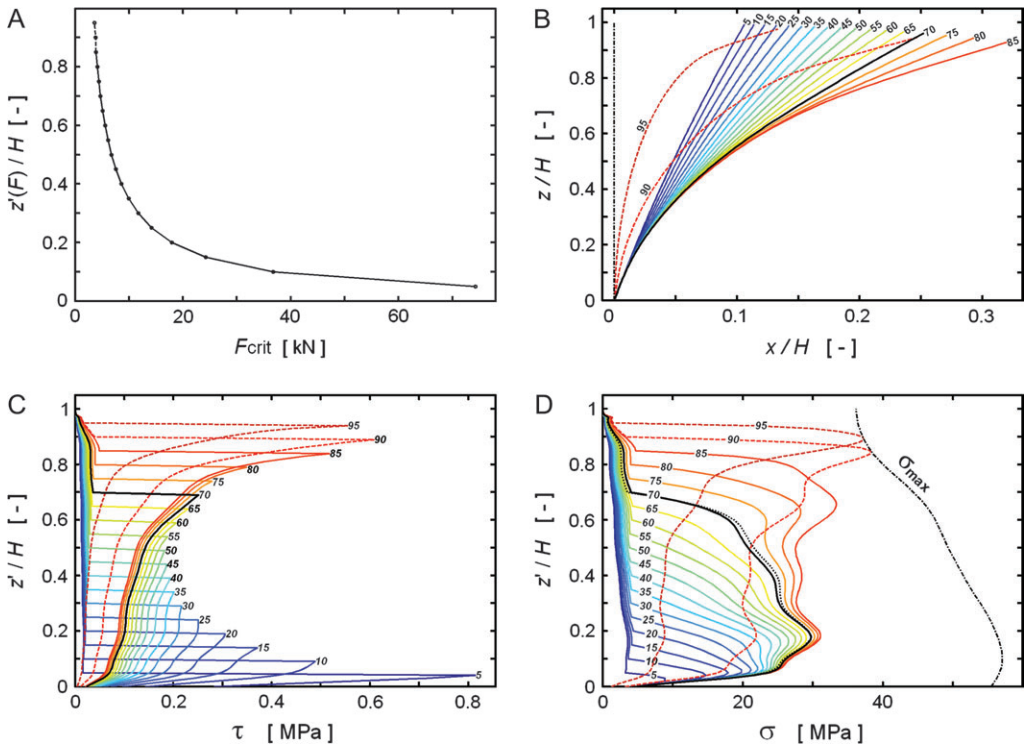

Fig. 3. (A) Values of critical lateral force F_{crit} as a function of the relative stem height of force application, $z'(F)/H$, for tree no. 15 in the unfrozen state with no snow load. Stem deflections (B), shear stress (τ) in the centre of the stem (C), and stem-bending stress (σ) (D) due to F_{crit} applied at $z'(F)/H$=5, 10, …, 95%. The dotted line indicates the σ due to the mean wind (1.7 m s^{-1}) magnified σ-wise to coincide with the $\sigma(z')$ at StEq(M^0_{max}). The dot-dash line (σ_{max}) is the stem-bending strength. Continuous lines refer to StEq(M^0_{max}) and dashed lines to StEq(σ_{max}). Heavy black lines (B–D) refer to the best 5%-multiple approximation for the relative height of the crown's area centre (z_{Cc}). Here z_{Cc}/H=68%≈70%.

to a certain height of force application (here $z'(F_{crit})/H$=87%), the tree uproots, i.e. StEq(M^0_{max}) applies (continuous lines). F_{crit} displays here a function of type $F_{crit} \sim z'^{b}$. Above this height, the tree fails in the stem, i.e. StEq(σ_{max}) applies (dashed lines), and $F_{crit}(z')$ decreases more strongly than indicated by $F_{crit} \sim z'^{b}$. The height at which this switch occurs depends on the degree of exploitation of bending stress capacity, $\sigma(z')/\sigma_{max}(z')$. The probability of shearing failure of the stem is highest when $F_{crit}(z')$ applies at the stem base (cf. Fig. 3C; Table 3). If F_{crit} applies above z'/H=0.05, the stem is more prone to bending failure than to shearing failure. Further, the $\sigma(z')$-curve due to F_{crit} and the $\sigma(z')$-curve due to the mean wind have similar shapes (Fig. 3D). The $\sigma(z')$-curve is the most similar in shape to the $\sigma_{max}(z')$-curve if F_{crit} applies just above the height of the crown's area centre, z_{Cc}. Compared with the unfrozen trees, $\sigma(z')/\sigma_{max}(z')$ was, as expected, lower if the stem was frozen, higher if both the stem and the soil were frozen, and much higher if only the soil was frozen. Furthermore, as expected, stem deflections were relatively larger for small than for big trees. For example, when F_{crit} was applied at z_{Cc}, the x- and z-wise tree-top deflections relative to H were at least 9% and 1%, respectively (tree 17, FrSt) and at most 63% and 30% (tree 11, 0_SL1), for all trees and combinations of tree state and snow load.

Stem-bending stress in relation to tree state and snow load

The spruces growing at the HE-site showed a low exploitation of their stem-bending capacity, $\sigma(z')/\sigma_{max}(z')$, when their M^0_{max} and the resulting uprooting was reached, i.e. at StEq(M^0_{max}). This is due to their relatively weak anchorage and strong stems. Consequently, the stem bending strength and the resulting stem failure, i.e. StEq(σ_{max}), was reached only if F was applied high up the stem. $\sigma(z')/\sigma_{max}(z')$ at StEq(M^0_{max}) was especially low for large trees (Fig. 4), meaning they were less likely to fail in the stem than small trees (Fig. 5). In fact, the largest trees, nos 16 and 17, were capable of achieving StEq(M^0_{max}) in all combinations of tree state and snow load even if F was applied above z_{Cc}. In contrast, the small HE-spruces in frozen soil failed in the stem if F was applied at z_{Cc} (e.g. no. 11 in Fig. 5E–G). As a consequence of the relatively weaker stem, the small HE-trees were generally more sensitive to snow load than the large trees (cf. Figs 4B, 5B). In fact, F_{crit} was very low for the trees nos 11–13 in the combination 0_SL2, independent of the height of application. This phenomenon of unstable equilibrium resulted in stem failure in the upper part of the crown at 0.70 < z'/H<0.95.

The spruces growing at the LE-site differed from those at the HE-site in that $\sigma(z')/\sigma_{max}(z')$ at StEq(M^0_{max}) was higher, meaning stem failure was more probable (cf. Fig. 6

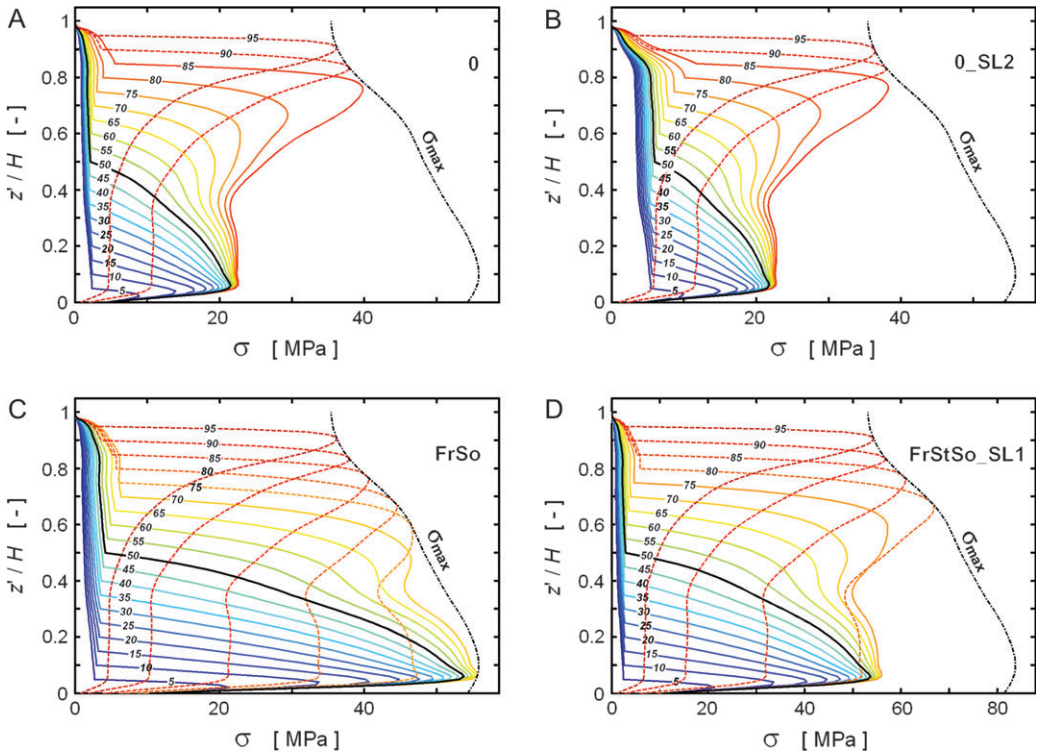

Fig. 4. Stem-bending stress (σ) due to F_{crit} for tree no. 16 in four combinations of tree state and snow load (cf. Table 4). Symbols are explained in Fig. 3.

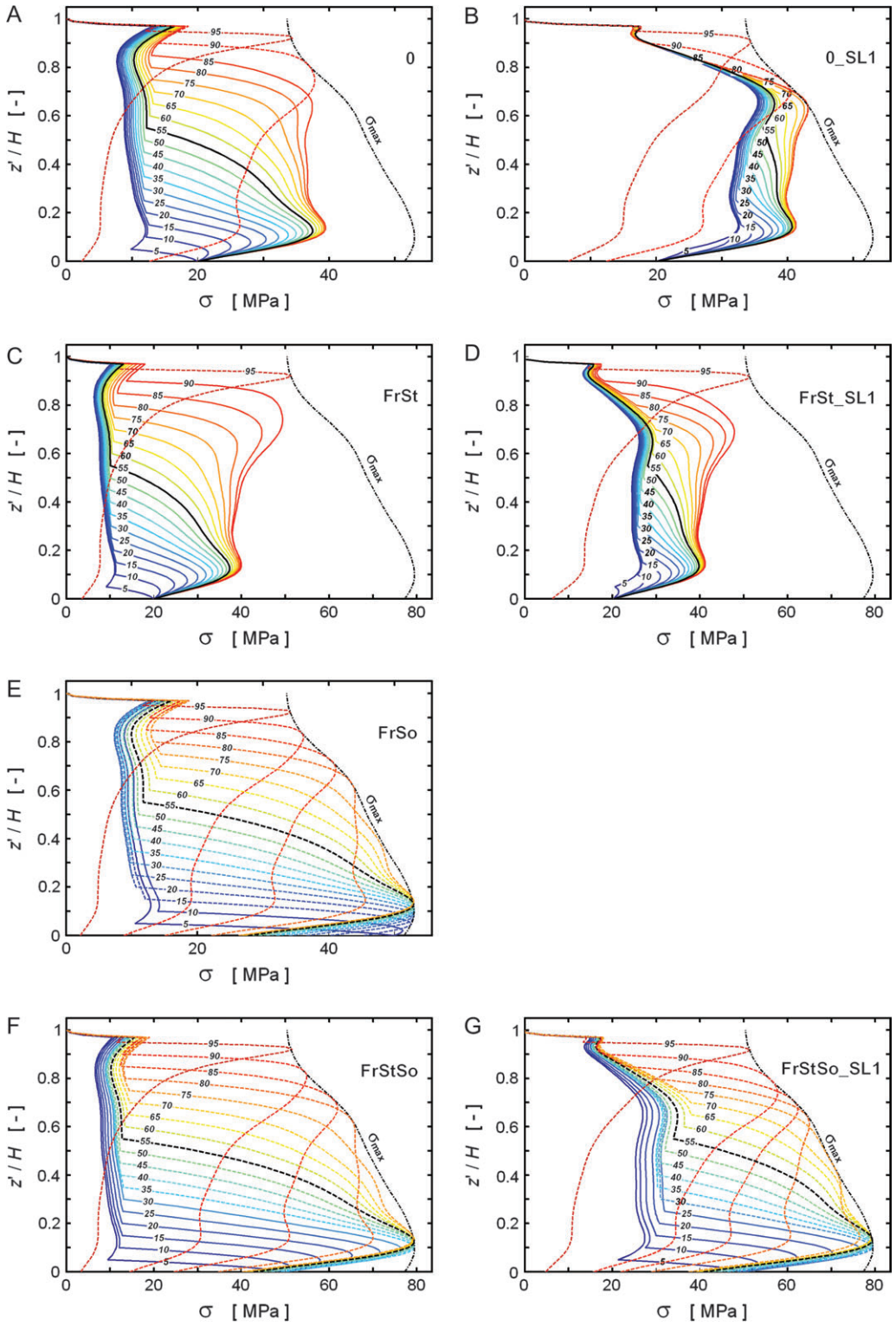

Fig. 5. Stem-bending stress (σ) due to F_{crit} for tree no. 11 in six tree-state/snow-load combinations (cf. Table 4). Symbols are explained in Fig. 3.

with Figs 4A and 5A). A further contrast with the HE-site was that the large LE-trees were more prone to stem failure than the small trees, with overall higher $\sigma(z')/\sigma_{max}(z')$ at StEq(M^0_{max}) (cf. Fig. 4B with Fig. 5B). Logically, in the tree-state and snow-load combination 0_SL1, the snow load caused overall higher $\sigma(z')/\sigma_{max}(z')$, just as it did with the HE-spruces. In the combination 0_SL2, the LE-spruces nos 22–25 failed in

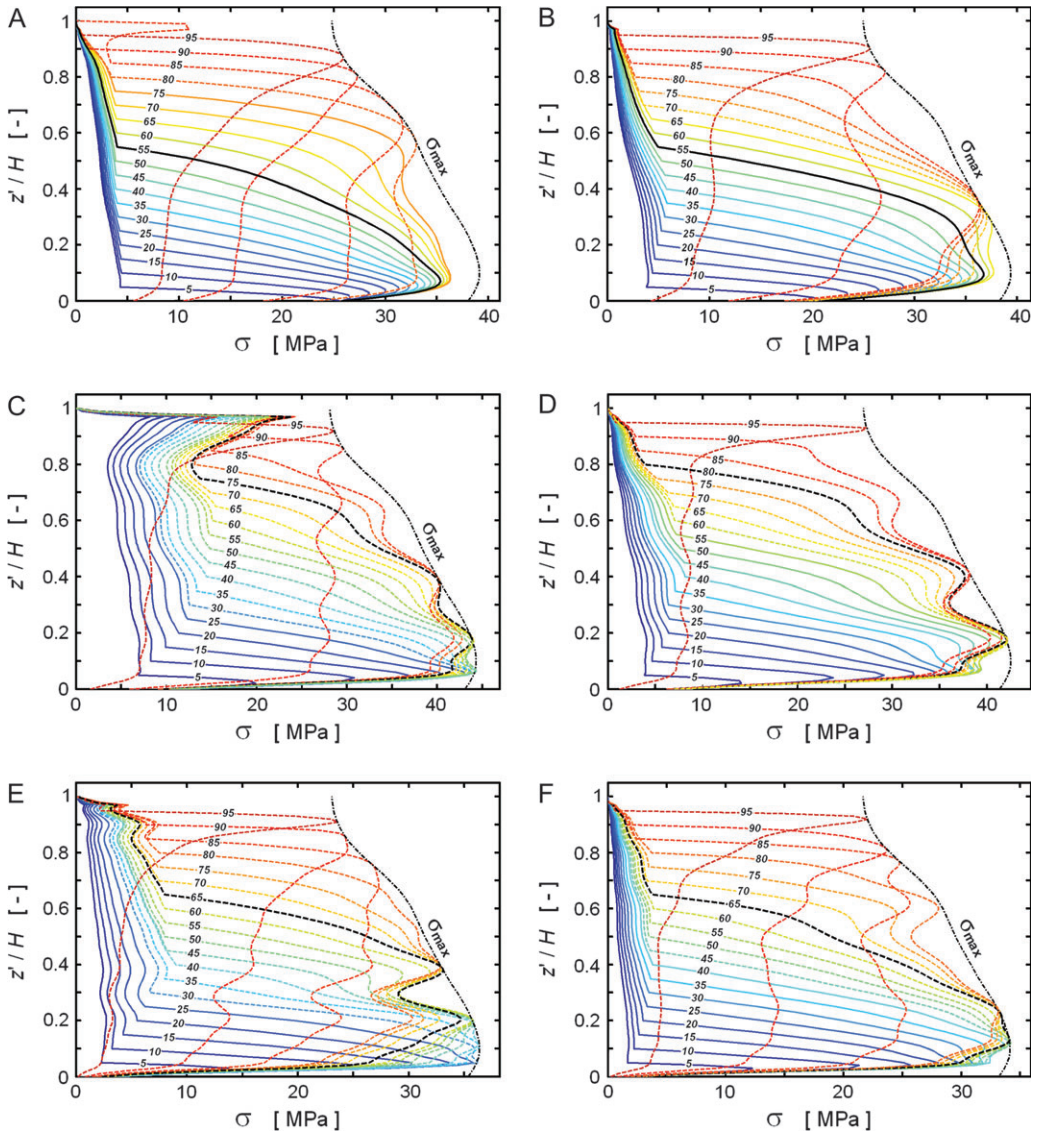

Fig. 6. Stem-bending stress (σ) due to F_{crit} in the normal tree-state/snow-load combination (0), for the trees nos 21–26 (A–F) with z_{Cc} close to z'/H=55, 55, 75, 80, 65, and 65% (heavier lines). StEq(M^0_{max} and σ_{max}) occurs with F_{crit} applied at about z'/H=77%, 66%, 29%, 56%, 25%, and 41% (A–F), where the continuous line shifts to a dashed line. Symbols are further explained in Fig. 3.

the stem at $0.50 < z'/H < 0.95$, with a very small F_{crit} required at any height (unstable equilibrium), whereas nos 21 and 26 showed simply generally higher $\sigma(z')/\sigma_{max}(z')$ at F_{crit} compared to 0_SL1.

Adaptation of stem and anchorage strengths to site-specific climate and loads

The HE-spruces displayed a well-balanced relation between the stem and the anchorage strengths when they were subjected to the combinations of tree-state and load application that can be expected during the year (Table 5). Thus, the simultaneous achievement of $M^0 = M^0_{max}$ and $\sigma(z') = \sigma_{max}(z')$, i.e. StEq($M^0_{max}$ and σ_{max}) was, for the unfrozen trees, often reached with F_{crit} at about $z' = 0.80H$ (i.e. 0.2–0.3H above z_{Cc}). This corresponds to the effective wind loading (cf. Discussion). If the soil and the stem were frozen, then $z'(F_{crit})$ at StEq(M^0_{max} and σ_{max}) was lower. With the smaller HE-trees, it shifted down towards the stem base, where, for example, pressure from gliding snow acts. In the combination 0_SL1, the HE-trees achieved StEq(M^0_{max} and σ_{max}) if F_{crit} was applied at the same z'/H-coordinate as the combination 0 or just a few per cent lower. In the combination 0_SL2 (nos 14–17), the corresponding downward shift was similar or just a few per cent more.

Most LE-trees (nos 21, 22, 24, and 26) achieved StEq(M^0_{max} and σ_{max}) with F_{crit} acting close to z_{Cc}. However, this balance was less evident than for the

Table 5. *Numerical data related to StEq(M^0_{max} and σ_{max}), i.e. the simultaneous achievement of $M^0 = M^0_{max}$ and $\sigma(z') = \sigma_{max}(z')$ due to the applied critical force F_{crit}, depending on the seasonal tree-state and snow load (cf. Table 4)*

If F_{crit} acts above the $z'(F_{crit})/H$ corresponding to StEq(M^0_{max} and σ_{max}), the stem fails. Otherwise the root–soil system fails (cf. legend in the table). M^0, turning moment acting on the root–soil system; M^0_{max}, maximum resistive M^0 of the root–soil system; $\sigma(z')$, stem-bending stress; $\sigma_{max}(z')$, stem-bending strength; z'/H, relative coordinate along the stem.

Tree no.	Seasonal tree state/snow load[a]						
	0	0 SL1	FrSt	FrSt SL1	FrSo	FrStSo	FrStSo SL1
11	0.85	0.80	0.90	0.90	0.10	0.30	0.25
	0.69	0.67	0.81	0.75	0.02	0.09	0.09
12	0.80	0.80	0.85	0.85	0.10	0.20	0.20
	0.61	0.61	0.78	0.79	0.04	0.07	0.07
13	0.85	0.80	0.85	0.85	0.15	0.75	0.75
	0.74	0.69	0.76	0.77	0.05	0.08	0.33
14	0.80	0.80	0.85	0.85	0.50	0.75	0.70
	0.69	0.69	0.75	0.75	0.23	0.62	0.30
15	0.85	0.85	0.90	0.90	0.35	0.80	0.80
	0.68	0.67	0.85	0.85	0.07	0.64	0.64
16	0.85	0.85	0.85	0.85	0.70	0.75	0.75
	0.78	0.78	0.78	0.78	0.06	0.61	0.61
17	0.80	0.80	0.85	0.85	0.70	0.75	0.75
	0.72	0.72	0.77	0.77	0.54	0.65	0.66
21	0.75	0.75					
	0.53	0.53					
22	0.65	0.55					
	0.30	0.27					
23	0.25	0.10					
	0.06	0.04					
24	0.55	0.45					
	0.17	0.17					
25	0.25	0.20					
	0.05	0.05					
26	0.40	0.35					
	0.11	0.11					

[a] Legend for each group of two numbers: $z'(F_{crit})/H \in$ StEq(M^0_{max} and σ_{max}); z'/H where $\sigma(z') = \sigma_{max}(z')$.

Table 6. *Numerical data related to the critical wind u_{crit}, depending on tree state and snow load (cf. Table 4)*

u_{crit} causes stem failure if $\max(\sigma/\sigma_{max}) = 1.00$, uprooting if $\max(\sigma/\sigma_{max}) < 1.00$, and both if the tree is in unstable equilibrium (*). σ, stem-bending stress; σ_{max}, stem bending strength (cf. legend in the table).

Tree no.	Seasonal tree state/snow load[a]						
	0	0 SL1	FrSt	FrSt SL1	FrSo	FrStSo	FrStSo SL1
11	9	4	8	5	21	18	14
	0.13	0.69	0.13	0.14	0.13	0.10	0.14
	0.71	0.90	0.47	0.50	1.00	1.00	1.00
12	15	8	13	8	33	28	21
	0.09	0.10	0.09	0.10	0.09	0.09	0.10
	0.76	0.79	0.50	0.52	1.00	1.00	1.00
13	13	8	11	8	32	28	20
	0.07	0.08	0.07	0.08	0.07	0.07	0.07
	0.57	0.59	0.38	0.38	1.00	1.00	1.00
14	15	13	14	12	38	33	25
	0.26	0.27	0.26	0.26	0.26	0.26	0.26
	0.42	0.44	0.28	0.28	1.00	0.69	0.71
15	22	16	18	15	46	42	31
	0.18	0.18	0.18	0.18	0.07	0.18	0.18
	0.53	0.54	0.35	0.35	1.00	0.87	0.89
16	19	16	17	15	45	39	30
	0.06	0.06	0.06	0.06	0.06	0.06	0.06
	0.39	0.39	0.26	0.26	0.97	0.64	0.65
17	32	24	25	20	57	53	41
	0.08	0.08	0.08	0.08	0.08	0.08	0.08
	0.27	0.27	0.18	0.18	0.68	0.45	0.45
21	22	19					
	0.07	0.07					
	0.91	0.92					
22	21	19					
	0.09	0.27					
	0.93	0.96					
23	20	11*					
	0.18	0.96					
	1.00	1.00					
24	34	24					
	0.19	0.42					
	1.00	1.00					
25	37	24					
	0.39	0.39					
	1.00	1.00					
26	41	31					
	0.14	0.23					
	1.00	1.00					

[a] Legend for each group of three numbers: u_{crit} [m s^{-1}]; z'/H for $\max(\sigma/\sigma_{max})$ [–]; $\max(\sigma/\sigma_{max})$ [–].

HE-trees, because the LE-trees sometimes lacked stem resistance. This was especially obvious with the LE-trees nos 23 and 25, which achieved StEq(M^0_{max} and σ_{max}) with F_{crit} acting at the lower part of the stem. In the combinations 0_SL1, the LE-trees achieved StEq(M^0_{max} and σ_{max}) if F_{crit} was applied at a z'/H-coordinate about 10% lower than in the combination 0. In the combination 0_SL2 (nos 21 and 26), the corresponding downward shift was 15%.

The critical speed of steady wind u_{crit} ranged between 4 m s^{-1} and 57 m s^{-1}, depending on the seasonal state of the tree and whether its crown was loaded with snow (Table 6). u_{crit} was best described by the social status of the tree in the stand (Table 1), with greater u_{crit} for more dominant trees, and then in turn by the tree size (DBH), by the site (LE or HE), or by the stand density. When described by the social status, u_{crit} was significantly higher (Wilcoxon signed-rank test, $P < 0.001$) at the LE-site than at the HE-site. Here, tree no. 23 appears weak and tree no. 12 strong in relation to their co-dominant positions. In general, the trees seem to have adapted their growth, and thus their stem and anchorage strength and crown size, reasonably well to the expected wind load. Subject to u_{crit}, the exploitation of the stem-bending stress capacity, σ/σ_{max}, was generally highest at $z' = 0.10$–$0.20H$, where the stems also exhibit their greatest $\sigma_{max}(z)$ (Fig. 3D). The LE-spruces tend to fail in the stem rather than uproot when exposed to u_{crit}, unlike the HE-spruces in unfrozen soil.

Degree of uniform exploitation of the stem-bending capacity, η

All HE- and LE-spruces display a mechanically adapted stem growth for lateral forces applied slightly above the area centre of the crown (Fig. 7). Hence, the HE-spruces exhibit high η-values if F acts on the upper crown ($0.6 < z'/H < 0.8$), similar to those of the LE-spruces ($0.6 < z'/H < 0.9$). In addition, the stems of the HE-spruces are well designed for bending due to forces acting on the lower part of the stem, up to approximately z'/H=0.20 (Fig. 7A), especially when loaded with snow (Fig. 7B). The general η-maximum along the upper stem is located higher for the LE-spruces than for the HE-spruces. Physically, this is a result of the LE-trees having relatively thicker stems along the upper half (Fig. 7D). If the crown of the HE-spruces is loaded with snow, the η-maximum is shifted downward (cf. Fig. 7A with B). A similar downward shift was observed for the LE-spruces.

The mechanically adapted stem growth is only weakly influenced by the tree states with frozen soil at the HE-site (Fig. 8), unlike those with snow load. Further, a stem's capacity (or need) to adapt its growth mechanically to different combinations of tree-state and snow load decreases with the age and size of the tree in terms of a less differentiated $\eta(z')$. The $\eta(z')$-curves of the LE-spruces with and without snow load showed a similar dependency on tree age and size.

Discussion

Model performance and potential sources of error when modelling stem deflections

There are several reasons for the differences between the parameterized and measured stem flexibility along the crown section of the stem. First, the branches induce local variations in grain orientation and stem diameter that influence the effective flexibility of the stem section. These variations were not taken into account. Second, the stem diameter was measured at larger intervals along the crown than along the stem base. Third, growth properties (*RW* and *Q*) were assessed in only two or three stem discs along the crown, which is a poor statistical base to predict the effective secant-modulus of elasticity E (governed by

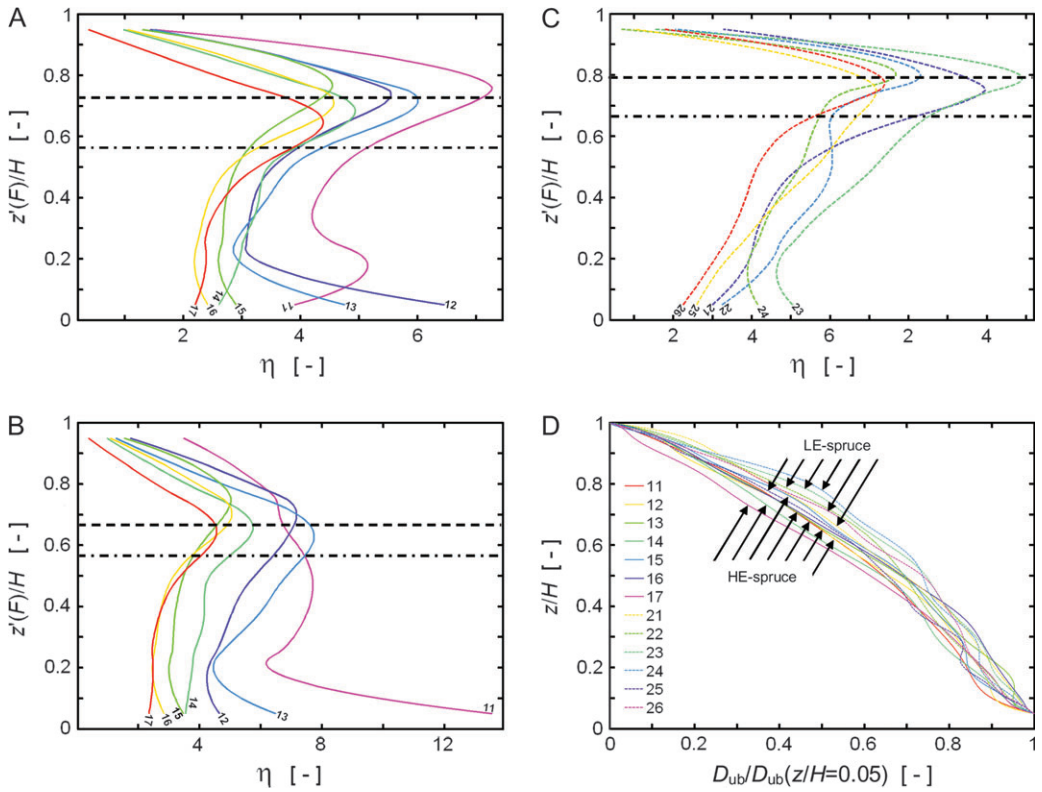

Fig. 7. (A–C) Site comparison of degrees of uniform exploitation of bending stress capacity, η, as a function of the relative coordinate along the stem z'/H at which the lateral force F acts: the HE-spruces in the tree-state/snow-load combination 0 and 0_SL1 (A, B) and LE-spruces in the combination 0 (C) (cf. Table 4). The η-maximum along the upper 80% of the tree (dashed lines) is shifted downwards if the crown is loaded with snow (A, B). The dot-dash lines indicate the location of the area centre of the crown. All horizontal lines are site medians. The inclined numbers indicate the tree no. (cf. Table 1 and Table 3). (D) The stem diameter under bark D_{ub} normalized by the D_{ub} at 5% stem height, as a function of the relative stem height z/H. The upper half of the stem is relatively thicker at the LE-site (dashed lines) than at the HE-site (continuous lines).

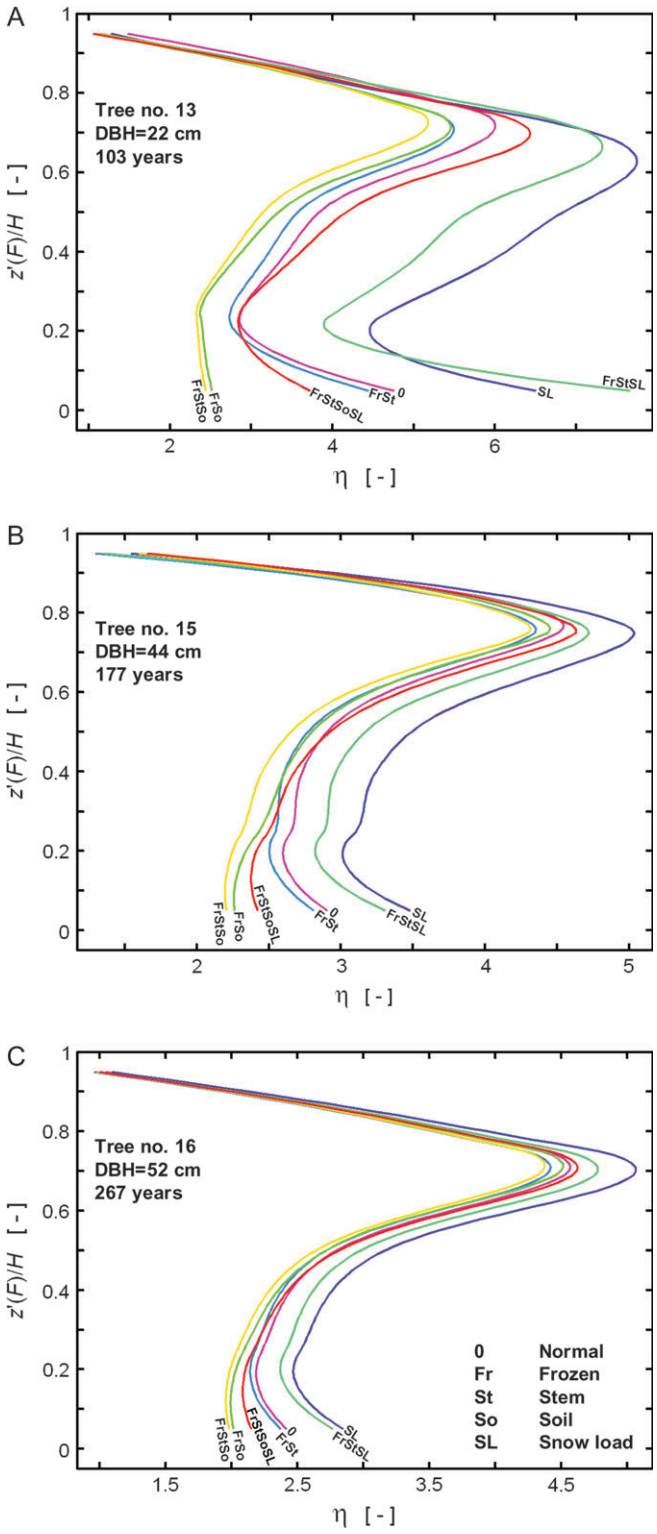

Fig. 8. Comparison of $\eta(z'(F)/H)$ among three spruces (A–C) of different sizes and cambial ages (at z=1.3 m) at the HE-site. DBH is the diameter at breast height and the axis symbols are explained in Fig. 7. Each curve corresponds to a particular combination of tree state and snow load (cf. legend in C). The snow load considered is SL1 (cf. Table 4).

Equation 1) here. Fourth, the predictive strength of E is low for the stem along the crown (Lundström *et al.*, 2008). Bending tests and investigations of the radial growth of fresh logs from the crown region are required to analyse and possibly reduce these sources of errors. However, the overall tree deflection is governed by the root–soil rotation and the bending of the stem base. The errors in flexibility along the crown section are therefore of minor importance when modelling the overall deflection of trees.

A geometric and material non-linear analysis can, unlike a linear analysis, describe *in situ* stem deflections precisely. Since this type of analysis requires non-linear experimental data, which are not always available, and more programming than if the analysis is made linear, it may be of interest to know when such precision is useful. When estimating critical lateral forces, a strict linear analysis will always overestimate the critical force (in the present case by up to 35%), especially if the crown is loaded with snow (possibly no additional force required for tree failure). A non-linear approach therefore seems adequate here as well as for failure analysis in general, for example when investigating the balance between the stem and anchorage strengths. As a comparison, the streamlining of the crown subject to wind, which is also a non-linear effect, reduces the effective drag force by up to 75% in strong wind (Equation 4). Unless the crown is loaded with heavy snow, crown streamlining is therefore the most important non-linear effect to consider in analysing tree reactions to wind. It is apparent that the spruces analysed are normally mechanically favoured by their overall flexibility, as demonstrated here by a 75%–35% = 40% higher F_{crit}.

Adaptation of stem and anchorage strength to tree states and loads

The strengths of the stem and the anchorage appear, in general, to be mutually best adapted to the prevailing combination of seasonal tree state and load, which at both sites is the wind on the unfrozen tree. The stem and anchorage strengths were also in balance for the HE-spruces in frozen soil subject to gliding or creeping snow (Table 5), especially for the smaller trees. The LE-spruces nos 23 and 25 were two exceptions to this pattern. Their growth seems to have been more strongly influenced by other criteria than the balance between the stem and anchorage strengths. Even so, the overall signs of mechanically adapted stem and anchorage strengths, which mean an adaptation of tree growth to acute loading, should be kept in mind when changes in the forest structure are planned.

The social status of the tree in the stand, the tree size, the site, and to some extent, the stand density seem, in turn, to govern the critical values of steady wind, u_{crit} (Table 6). This indicates that the tree adapts, through appropriate growth allocation, its stem and anchorage

strengths as well as its crown size to the wind pressure. In this study, the steady wind and a uniform wind pressure on the entire crown were used as a basis for comparing the u_{crit} of the trees. Evidently, a tree will also experience (i) gusts due to the wind turbulence (Holbo *et al*., 1980), (ii) dynamic, structural amplification due to tree-wind resonance (Peltola, 1996; SIA, 2006), (iii) varying types of wind profile in the canopy (Raupach, 1994; Lo, 1995) depending on the local topology and stand structure, and possibly (iv) torsion (Mayer, 1985). When relating u_{crit} to standard 10-min-wind measurements, the two first effects tend to counterbalance the third. It is, however, obvious that predictions of wind-induced tree failure will require additional and more specific measurements than those made in the present study. Nevertheless, this analysis clearly shows that the studied trees in frozen soil will never fail due to wind load alone, and that the trees with unfrozen stem and soil and snow-loaded crowns are at greatest risk of wind failure. The HE-trees are accustomed to frost (note that light frost is more frequent than 'Fr' in Table 4) and appear to allocate growth to the anchorage and the stem in accordance. In fact, they seem to rely on their anchorage and stem strengthening when the crown is loaded with snow, which is another sign of site-specific mechanical growth adaptation.

Field observations at the HE-site over the last few decades (H Hefti, municipal forester at the HE site, personal communication) reveal only a few tree failures. These were mainly due to local Foehn-storms, small slabs of gliding snow, and rare tree-top failure due to snow-loaded crowns. In comparison, more frequent tree failures due to winter storms were observed at the LE-site, of which about one-third were stem and two-thirds root–soil failure (B Blöchliger, municipal forester at the LE-site, personal communication). These observations are in line with the model simulations in this study.

Degree of uniform exploitation of the stem-bending capacity, η

Stem thigmomorphogenesis reflects the local prevailing seasonal combination of tree state and load. In fact, the degree of uniform exploitation of bending stress capacity $\eta(z')$ (Equation 8) shows that both the taper and the material properties of the stem mechanically adapt to frequent complex loading, independent of the growth situation. This is especially true for young trees (Fig. 8). The general maxima of $\eta(z')$ of about 0.75 (Fig. 7) shows that the stem adapts its growth to the effectively induced wind load, just like the strengths of the stem and of the root–soil system. Actually, the effective height of equivalent wind-force application $z'(F)$ on the crown could be estimated to 20–25% above the crown's area centre if the crown's area was considered by segments of height in Equation 7 and an approximate mean wind profile in the canopy was assumed (on the basis of Zoumakis, 1993; Raupach, 1994).

In terms of stem thigmomorphogenesis, the thicker stems of the LE-spruces along the crown section of the stem, and thus the slightly higher located $\eta(z')$-maxima for the LE- compared to the HE-spruces, could be a result of differences in the wind pressure profiles, with relatively higher pressures close to the tree tops at the LE-site. Concerning the observed response in stem growth to the prevailing load combination, the snow load SL1 is an exception. Although the tree crown is mostly not covered with snow, the stem seems to 'remember' this critical additional load and adapts its growth accordingly. The downward shift in general $\eta(z')$-maxima for trees with snow-loaded crowns seems natural, since the equivalent wind force acting on the crown is likely to shift downward if the branches are loaded with snow. This interpretation is supported by the fact that the application height of F_{crit} at StEq($M^0_{max}$and σ_{max}) was also shifted downward if the crown was loaded with snow.

It is known that trees also exhibit stem failure due to shearing (Mattheck and Breloer, 1994), but no signs of stem thigmomorphogenesis due to shear stresses were found. To ascertain this will require a shear-stress modelling with more detail than could be included in this study. Nevertheless, the formulation of the degree of uniform exploitation of a tree's stem-bending stress capacity presented here provides further strong evidence that tree stems are able to adapt their growth mechanically.

This study covers numerous tree and climate parameters, with an emphasis on drawing general conclusions rather than doing a detailed analysis of the spatiotemporal growth response of spruce to mechanical stress. For more insight into the thigmomorphogenesis of Norway spruce, it would be worthwhile analysing how specific growth processes develop in detail under the influence of variable mechanical stress and climatic conditions.

Acknowledgements

We thank Silvia Dingwall for revising the text and the anonymous reviewer for constructive comments.

Appendix

List of symbols and notations and their definitions and units used in the study

Notation	Description	Unit
A	Area of the stem cross-section	m^2
B	Bark thickness	m, mm
D, $D_{ub;\ x,\ y,\ 05}$	Stem diameter over and under bark; reference to x-direction, y-direction, and to 5% tree height (cf. Table 2)	m, mm
DBH	Stem diameter over bark at breast height (z=1.3 m)	m, cm
E	Secant-modulus of stem bending elasticity $= \sigma/\varepsilon$	GPa
ε	Stem-bending strain (without the contribution from shear deformation)	–

Continued

Continued

Notation	Description	Unit
F ; F_{init}; F_{crit}	Force applied on the tree in the x-direction; F initially applied; critical F, causing stem-bending failure ($\sigma=\sigma_{max}$), or tree uprooting ($M^0 \approx M^0_{max}$), or both ($M^0_{max}$and σ_{max}) simultaneously	N
ϕ	Rotation around the y-axis of the root-soil system	rad, °
G	Secant-modulus of shearing elasticity along the stem	MPa
γ	Stem-shear strain along the stem	–
H	Tree height	m
η	Degree of uniform exploitation of the stem-bending capacity (cf. Equation 8)	–
HE, LE	High-elevation site, low-elevation site	
M	Turning moment around the y-axis of the stem section	MPa
M^0; M^0_{max}	Turning moment around the y-axis of the root–soil system; maximum resistive M^0	MPa
MOE	Secant-modulus of stem bending elasticity defined at $\sigma=0.4\sigma_{max}$	GPa
N	Normal force (along the stem)	N
Q	Knottiness (relative frequency of knots) in the stem cross-section	–
r	Radial coordinate of the stem, ranging from the stem centre to the bark ($D_0/2$)	m
RW; $_{i,o}$	Width of annual rings; reference to the mean of the inner 75% radial part of the stem cross-section and to the mean of the remaining outer part	mm
σ, σ_{max}	Bending stress and strength of the stem cross-section	MPa
SL1, SL2	Snow load on the crown m^{-1} height (1= moderate; 2=heavy, cf. Table 4 and the text)	kg m^{-1}
StEq	Static equilibrium for the tree model when subjected to F_{crit} (cf. explanation of F_{crit} above)	
SWE	Snow-water equivalent precipitation relating to the amount of snow	mm
τ, τ_{max}	Shear stress and strength of the stem section in the direction along the stem	MPa
u; u_{crit}	Wind speed; critical u causing stem-bending failure ($\sigma=\sigma_{max}$) or tree uprooting ($M^0 \approx M^0_{max}$)	m s^{-1}
V	Shear force (across the stem)	N
x, y, z	Global (Cartesian) coordinates of the tree: origin at stem base; x=horizontal stem deflection; z=height above origin (cf. Fig. 1)	m
x', z'	Local coordinates of the deflecting stem; x'=sideway deflection of each stem element; z'=coordinate along the deflecting stem, ranging from 0 to H (cf. Fig. 1).	m
z_{Cc}	Height of the crown's area centre	m

References

Ancelin P, Fourcaud T, Lac P. 2004. Modelling the biomechanical behaviour of growing trees at the forest stand scale. Part 1. Development of an incremental Transfer Matrix Method and application to simplified tree structures. *Annals of Forest Science* **61,** 263–275.

Andersland OB, Ladanyi B. 2004. *Frozen ground engineering*. 2. Hoboken, NJ: Wiley.

Bründl M. 1997. *Snow interception and meltwater transport in subalpine forests*. Monograph 12271. Zürich: ETH.

Chiatante D, Scippa SG, Di Iorio A, Sarnataro M. 2002. The influence of steep slopes on root system development. *Journal of Plant Growth Regulation* **21,** 247–260.

Cook RD, Malkus DS, Plesha ME. 2002. *Concepts and applications of finite element analysis*. 4. New York: Wiley.

Dean TJ, Roberts SD, Gilmore DW, Maguire DA, Long JN, O'Hara KL, Seymour RS. 2002. An evaluation of the uniform stress hypothesis based on stem geometry in selected North American conifers. *Trees—Structure and Function* **16,** 559–568.

Di Iorio A, Lasserre B, Scippa GS, Chiatante D. 2005. Root system architecture of *Quercus pubescens* trees growing on different sloping conditions. *Annals of Botany* **95,** 351–361.

Dobbertin M, Hug C, Schwyzer A. 1997. *Sanasilva Inventory Field Manual*. WSL, 18(57).

Holbo HR, Corbett TC, Horton PJ. 1980. Aeromechanical behavior of selected Douglas-Fir. *Agricultural Meteorology* **21,** 81–91.

Jaffe MJ. 1973. Thigmomorphogenesis: The response of plant growth and development to mechanical stimulation. *Planta* **114,** 143–157.

Kalberer M. 2007. *Quantification and optimization of the forest protection against rock falls*. Monograph. Freiburg: University of Freiburg.

Kollmann FFP. 1968. *Principles of wood science and technology* Vol. 1 *Solid wood*. Berlin: Springer.

Laasasenaho J, Melkas T, Alden S. 2005. Modelling bark thickness of *Picea abies* with taper curves. *Forest Ecology and Management* **206,** 35–47.

Lo AKF. 1995. Determination of zero-plane displacement and roughness length of a forest canopy using profiles of limited height. *Boundary-Layer Meteorology* **75,** 381–402.

Lundström T, Heiz U, Stoffel M, Stöckli V. 2007*a*. Fresh-wood bending: linking the mechanical and growth properties of a Norway spruce stem. *Tree Physiology* **27,** 1229–1241.

Lundström T, Jonas T, Stöckli V, Ammann W. 2007*b*. Anchorage of mature conifer: resistive turning moment, root–soil plate geometry and orientation of root growth. *Tree Physiology* **27,** 1217–1227.

Lundström T, Jonsson MJ, Kalberer M. 2007*c*. The root–soil system of Norway spruce subjected to turning moment: resistance as a function of rotation. *Plant and Soil* **300,** 35–49.

Lundström T, Stoffel M, Stöckli V. 2008. Fresh-stem bending of silver fir and Norway spruce. *Tree Physiology* **28,** 355–366.

Mattheck C, Breloer H. 1994. *The body language of trees: a handbook for failure analysis*. London: HMSO.

Mayer H. 1985. *Baumschwingungen und Sturmgefährdung des Waldes*. München: 51: Universität München, Meteorologisches Institut.

Meng SX, Lieffers VJ, Reid DEB, Rudnicki M, Silins U, Jin M. 2006. Reducing stem bending increases the height growth of tall pines. *Journal of Experimental Botany* **57,** 3175–3182.

Milne R. 1991. Dynamics of swaying of *Picea sitchensis*. *Tree Physiology* **9,** 383–399.

Morgan J, Cannell MGR. 1987. Structural analysis of tree trunks and branches: tapered cantilever beams subject to large deflections under complex loading. *Tree Physiology* **3,** 365–374.

Morgan J, Cannell MGR. 1994. Shape of tree stems: a reexamination of the uniform stress hypothesis. *Tree Physiology* **14,** 49–62.

Moulia B, Coutand C, Lenne C. 2006. Posture control and skeletal mechanical acclimation in terrestrial plants: implications for mechanical modeling of plant architecture. *American Journal of Botany* **93,** 1477–1489.

Nicoll BC, Ray D. 1996. Adaptive growth of tree root systems in response to wind action and site conditions. *Tree Physiology* **16,** 891–898.

Niemz P. 1993. *Physik des Holzes und der Holzwerkstoffe Holz: Anatomie, Chemie, Physik* Vol. III. DRW-Verlag.

Peltola H. 1996. Swaying of trees in response to wind and thinning in a stand of Scots pine. *Boundary-Layer Meteorology* **77,** 285–304.

Peltola H, Kellomäki S, Hassinen A, Granander M. 2000. Mechanical stability of Scots pine, Norway spruce and birch: an analysis of tree-pulling experiments in Finland. *Forest Ecology and Management* **135,** 143–153.

Peltola H, Nykanen ML, Kellomaki S. 1997. Model computations on the critical combination of snow loading and windspeed for snow damage of Scots pine, Norway spruce and Birch sp. at stand edge. *Forest Ecology and Management* **95,** 229–241.

Pomeroy JW, Gray DM. 1995. *Snowcover accumulation, relocation and management*. National Hydrology Research Institute science report. Saskatoon, Saskatchewan, Canada: National Hydrology Research Institute.

Raupach MR. 1994. Simplified expressions for vegetation roughness length and zero-plane displacement as functions of canopy height and area index. *Boundary-Layer Meteorology* **71,** 211–216.

Schweingruber FH. 1996. *Tree rings and environment. Dendroecology*. Bern: Haupt.

SIA. 2006. *Wind*. D 0188, Zurich: Schweizerischer Ingenieur- und Architektenverein (SIA).

Silins U, Lieffers VJ, Bach L. 2000. The effect of temperature on mechanical properties of standing lodgepole pine trees. *Trees–Structure and function* **14,** 424–428.

Stadler DC, Bründl M, Schneebeli M, Meyer-Grass M, Flühler H. 1998. *Hydrologische Prozesse im subalpinen Wald im Winter*. Schlussbericht/NFP 31. Zürich VDF; Hochschulverlag an der ETH.

Strobel T. 1978. *Schneeinterzeption in Fichtenbeständen in den Voralpen des Kantons Schwyz*. Davos, Switzerland: International Seminar on Mountain, Forests and Avalanches, 63–79.

Telewski FW. 1995. Wind-induced physiologial and developmental responses in trees. In: Coutts M, Grace J, eds. *Wind and trees*. Cambridge: Cambridge University Press, 241–263.

Telewski FW. 2006. A unified hypothesis of mechanoperception in plants. *American Journal of Botany* **93,** 1466–1476.

Wood CJ. 1995. Understanding wind forces on trees. In: Coutts MP, Grace J, eds. *Wind and trees*. Cambridge: Cambridge University Press, 133–164.

Yang YB, Yang YT, Su HH. 2005. Behavior of the tree branches, trunk, and root anchorage by non-linear finite element analysis. *Advances in Structural Engineering* **8,** 1–14.

Ylinen A. 1952. Über die mechanische Schaftformtheorie der Bäume. *Silva Fennica* **76,** 1–52.

Zoumakis NM. 1993. Estimating the zero-plane displacement and roughness length for tall vegetation and forest canopies using semi-empirical wind profiles. *Journal of Applied Meteorology* **32,** 574–579.

Zweifel R, Hasler R. 2000. Frost-induced reversible shrinkage of bark of mature subalpine conifers. *Agricultural and Forest Meteorology* **102,** 213–222.